Available online at www.sciencedirect.com
ScienceDirect
Scripta Materialia 59 (2008) 471–474
Scripta MATERIALIA
www.elsevier.com/locate/scriptamat

On the initial microstructure of metallic micropillars

R. Maaß, S. Van Petegem, J. Zimmermann, C.N. Borca and H. Van Swygenhoven*

Paul Scherrer Institute, CH-5232 Villigen, Switzerland

Received 5 April 2008; accepted 20 April 2008
Available online 1 May 2008

White beam Laue microdiffraction has been performed to investigate the initial microstructure of undeformed Au, Ni, Cu, and NiTi micropillars fabricated by focused ion beam milling. Various microstructural features have been shown, from which it is known that they contribute to classical hardening.

Keywords: Micropillars; Plasticity; Microstructure; Defects; Single crystals

Compression of micron-sized pillars [1] has shown enhanced strengthening in face-centered cubic [2,3] and body-centered cubic [4] single crystals when the pillar diameter is reduced to below 20 μm. From the published mechanical data, however, it is evident that a scatter as high as 100% can exist for nominally identical samples [5,6], which can in part been explained by the stochastic nature of plasticity [7,8]. In these approaches it is assumed that the initial pillar structure does not contain microstructural features classically known to result in hardening and that the pillars are strain-gradient-free single crystals. However, white beam Laue diffraction has demonstrated that this is not always the case: the first example is an Au pillar with a pre-existing strong strain gradient that rules the selection of the slip system [9]; the second is an Ni pillar containing a low-angle grain boundary [10]. Here, we report on the initial microstructure prior to deformation of 14 single crystal and two multi-grained pillars, classified into six groups according to chemical substance and crystallographic orientation. Laue diffraction reveals several microstructural features that within classical crystal plasticity are known to result in hardening, ranging from misorientations at the pillar base to twin defects and in homogeneous strain gradients in the body of the pillars. In two samples containing multiple grains, strain gradients were also found in each of the individual grains.

Table 1 shows the chemical composition, orientation, and diameter of the 16 investigated pillars tabulated into six groups. Most of the pillars were made from the same material as reported in Ref. [10] for Ni, Ref. [11] for Cu, Ref. [9] for Au⟨346⟩, Ref. [12] for NiTi and Ref. [13] for sputtered Au. The Au⟨123⟩ samples were made using the same procedure as the Au⟨346⟩ samples in Ref. [14]. The initial bulk material was a commercially available single crystal, except for the sputtered Au and the Au⟨346⟩. Au⟨346⟩ pillars were cut out of larger grains in an annealed foil, as was done in Refs. [9,14]. All samples within each group were made out of the same bulk piece, with a typical pillar-to-pillar distance of 50–100 μm, except the Cu samples, which were focused ion beam (FIB) milled from individual single crystal bulk pieces.

The FIB milling conditions were different between all the sample groups, but the same within each: for instance, final current densities of 50 pA were applied for Au⟨123⟩ and Au⟨346⟩, 100 pA for the Cu pillars and 1 nA for the Ni pillars, whereas the acceleration voltage was 30 keV in all cases. White beam Laue diffraction was performed in transmission at the MicroXAS beam line of the Swiss Light Source with a microfocused white X-ray beam having an energy distribution ranging from 2 to 22 keV and a beam size between 0.8 and 2 μm in the focal plane. Further details on the experimental technique are given in the online material of Ref. [9]. For each group of pillars a reference Laue pattern of a Si wafer was recorded under the same conditions, which allows monitoring of the resolution function and verification of the calibration parameters.

The range in photon energy used in white beam Laue diffraction allows lattice curvatures and small angular misorientations to be detected without the need for a rocking curve. For instance, excess dislocations of one sign generating a lattice curvature results in a streaked

* Corresponding author. E-mail: helena.vs@psi.ch

1359-6462/$ - see front matter © 2008 Acta Materialia Inc. Published by Elsevier Ltd. All rights reserved.
doi:10.1016/j.scriptamat.2008.04.034

Table 1. Sample groups with their chemical composition, vertical crystal axis orientation and corresponding pillar diameters

Group	Chemical composition	Crystallographic orientation	Diameter (μm)
1	Au	⟨123⟩	3 × 2.0, 3.0, 4.0
2	Au	⟨346⟩	0.8, 3.0
3	Cu	⟨421⟩	5.0, 5.4
4	Ni	⟨123⟩	2 × 8
5	Ni–50.9 at.%Ti	⟨210⟩	2.3, 2.8, 3.0
6	Au	Sputtered ⟨111⟩	0.9, 1.1

Laue diffraction peak. The angular width of such a streaked peak can then be used to estimate the radius of lattice curvature, which is proportional to the excess dislocation density times the Burgers vector [15,16]. On the other hand, when geometrical necessary dislocations (GNDs) organize into geometrically necessary boundaries (GNBs) to reduce the stored energy, the Laue spot will split, reflecting the contributions from two separate crystal volumes [17]. The above simple approach has been applied to estimate the dislocation densities from the (*hkl*) reflection showing the largest streak or split, assuming the existence of only one slip system populated with an excess dislocation density.

In several of the investigated samples, misorientations (GNBs) were observed at the pillar base. In the group of the Au⟨123⟩ samples, two pillars with a peak split in the lower part were identified by mapping the sample with Laue patterns along its vertical axis. Figure 1a shows a scanning electron microscopy (SEM) image taken under a 66° tilt angle of a 3 μm Au⟨123⟩ pillar with a height of 8 μm, that is, an aspect ratio of 1:2.7. The Laue diffraction intensity of the (2-2-2) reflection is given in Figure 1b–e for different positions of the incoming X-ray beam along the pillar axis. Note that all experiments are performed in transmission geometry with the incoming beam perpendicular to the pillar axis. At position 4 (Fig. 1e) the Laue pattern corresponds with the single crystal orientation and none of the diffraction peaks show peak splitting. When scanning downwards, the intensity distribution of the Laue peaks evidence a transition from a single diffraction peak towards a split peak at the pillar base, that is, Figure 1c taken at position 2. At position 3, that is more than half-way along the pillar length or 5 μm above the pillar-base, the smeared out intensities of the overlapping peaks show that the misorientation extends from the base well into the pillar and that only the upper part of the pillar corresponds with a single crystal orientation.

From the splitting of the Laue peaks at position 2 (8 μm from the pillar's top) a misorientation angle of 0.07° is derived, which is equal to a GND density of $\sim 2.8 \times 10^{12}\,\mathrm{m}^{-2}$ in the GNBs present in the probed volume. A similar split was observed in one of the 2 μm Au⟨123⟩ samples, whereas the other Au pillars of the same group did not exhibit any misorientations at the pillar base. Peak splitting with a magnitude of $0.07°/4.9 \times 10^{12}\,\mathrm{m}^{-2}$ was also observed at the base of the 8 μm Ni sample (called Ni B). In particular cases, peak splitting was even observed in the center of the pillar. For example, in the 0.8 μm Au⟨346⟩ pillar and the 2.3 μm NiTi sample, splitting angles and corresponding GND densities of $0.42°/2.5 \times 10^{13}\,\mathrm{m}^{-2}$ (Au⟨346⟩) and $0.23°/1.8 \times 10^{13}\,\mathrm{m}^{-2}$ (NiTi) were found. The intensity distribution of the NiTi $(00\bar{2})$ peak and the Au⟨346⟩ $(\bar{2}2\bar{2})$ at half the pillar height are displayed in Figure 2a and b. In addition to the substructure in the 0.8 μm Au⟨346⟩ pillar, it was found that the pillar itself was rotated relative to the substrate by 0.72°, compared with the vertical axis obtained from fits performed on the entire Laue pattern from the pillar base and taken at half the pillar height. Figure 2b shows that both the substrate and the pillar $(\bar{2}2\bar{2})$ signal are shifted by 0.48° with respect to each other. Due to similar pillar height and beam size, a substrate signal is also recorded at half the pillar height. Note that the pillar and its substrate were machined out of a single grain, which is why the entire pillar is rotated with respect to the orientation of the substrate. Pre-existing GNBs will contribute as a Hall–Petch-like hardening factor according to $\tau_f = K(Gb)^{0.5}/(D_{GNB})^{0.5}$, where τ_f is the flow tress, K is a constant, G is the shear modulus, b is the Burgers vector and D_{GNB} is the spacing of the GNBs [18]. Moreover, a misorientation in the lower pillar part will hinder dislocation escape into the base and result in back stresses similar to a decaying stress field under load due to the tapering of the pillar, which also artificially hardens the sample. Misfits at the pillar base complicate the imposed boundary conditions of the compression test and therefore also the comparison of pillars with and without misfits.

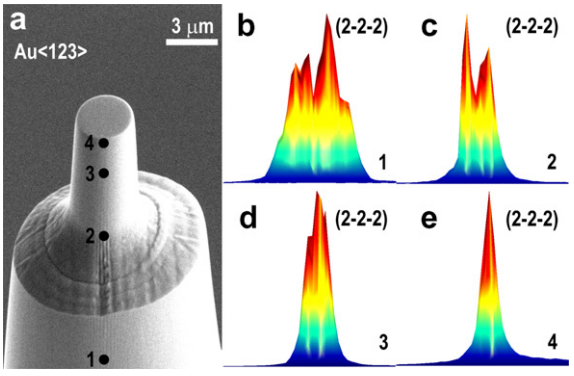

Figure 1. An SEM image of a 3 μm Au⟨123⟩ pillar, with split peaks along its vertical axis shown in Figure 2b–e; position 3 is 5 μm above the pillar–base transition.

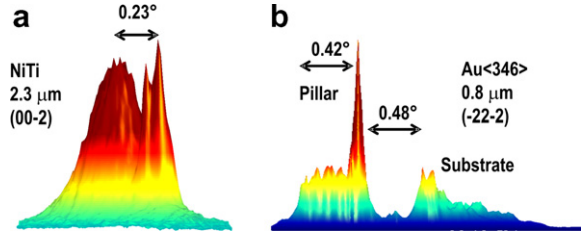

Figure 2. (a) Split (00-2) NiTi peak and (b) split $(\bar{2}2\bar{2})$ Au⟨346⟩ peak of the 800 nm pillar and a 0.48° misorientation between the pillar and the substrate, which were initially of identical orientation.

For several samples anisotropic peak shapes were observed that were indicative of strain gradients. This was particularly true for the smaller pillars. For the two large Cu pillars and for one of the 8 μm Ni (Ni A) pillars no significant peak asymmetries could be detected. Figure 3f and g displays the $(\bar{1}\,\bar{3}\,1)$ Ni and the $(1\,\bar{3}\,\bar{1})$ Cu peak, respectively. The peak shapes were fitted by a two-dimensional Pearson VII function. We find for the full-width at half-maximum (FWHM) $0.06°\theta/0.06°\psi$ (Ni) and $0.07°\theta/0.06°\psi$ (Cu), where θ and ψ are defined as the radial and azimuthal direction, respectively. This is similar to the values obtained for the Si reference wafer ($0.06°\theta/0.06°\psi$).

For smaller pillars, however, clear peak asymmetries were found. Here the minor directions from the Pearson VII fits are comparable to those from Si, whereas the major peak axis shows large gradients. This was the case for two of the three Au⟨1 2 3⟩ pillars and NiTi samples. Figure 3a and b shows the $(2\bar{2}\bar{2})$ reflections of the 2 μm Au⟨1 2 3⟩ pillars, called A and B. It is obvious that pillar B contains a more pronounced strain gradient than pillar A. A curvature of 0.20° could be calculated from a line scan in the theta direction that corresponds to an initial excess dislocation content of the order of 1.5×10^{13} m^{-2} using the Nye relationship [15]. To calculate the curvature, it was assumed that the Si peak width contains both the beam divergence of 0.2 mrad and the instrumental broadening function. The peak widths of Si and Au were then deconvoluted to determine the Au curvature. All NiTi samples show a strain gradient, albeit to different extents, as shown in Figure 3c and d for the $(00\bar{2})$ reflection of the 2.8 and 3.0 μm pillars, respectively. In total, 6 of the 12 samples with diameters smaller than 5 μm show strain gradients reflected in asymmetric peaks. On the basis of strain-gradient-based plasticity, a Taylor-like flow stress, including the GND density, has been formulated as $\tau_f = \alpha\, Gb(\rho_{SSD} + \rho_{GND})^{0.5}$, with α a constant, G and b as above, ρ_{SSD} the statistically stored dislocation density and ρ_{GND} the GND density [19], which clearly demonstrates that the presence of GNDs introduces a significant hardening factor.

In addition to the regularly found strain gradients in the pillar bodies and misorientations at the pillar base and even in the pillar, other types of defects were found, albeit less frequently. Earlier investigations have, for instance, shown the strengthening effect of a low angle boundary in Ni⟨0 6 8⟩ [10]. In the present study, a twin boundary in a 3 μm Au⟨3 4 6⟩ pillar with a rotation of 60° around the $[\bar{1}\,1\,1]$ axis was found, as evidenced by two partly overlapping sets of Laue peaks on the diffraction pattern. Figure 4 displays the $[\bar{1}\,1\,1]$ twin boundary sketched in the SEM image of the sample and the corresponding Laue pattern with the twin peaks labeled as $(hkl)t$. Molecular dynamics simulations have shown the strengthening effect in gold pillars via Lomer–Cotrell locks at the twin boundary [20].

Finally, we investigated two Au pillars that were provided to us by Budiman et al. [13] and made by FIB from an Au film sputtered on a [0 0 1]-Cr substrate. For both samples investigated, the Laue patterns revealed the presence of four individual grains, each oriented out of plane closely to the [1 1 1] growth direction with an angular deviation of ±3.8°. Rotating the orientation solution for grain 1 around the vertical grain axis (i.e. in-plane) by +30°, +60° or −30° results in the Laue patterns of grains 2, 4 and 3, respectively, thereby fulfilling the condition that the Au⟨1 1 0⟩ direction aligns with the Cr⟨1 0 0⟩ direction according to the orientation relation determined in Ref. [13]. A Laue pattern for the sputtered 1.1 μm pillar is shown in the upper part of Figure 5, together with an SEM image of the sample taken in beam direction. In Figure 5 all non-indexed reflections belong to the Cr substrate.

For all the individual grains, all Laue reflections show peak asymmetries, including peak streaking and/or peak splitting, as demonstrated in Figure 5. For instance, the peak splitting observed in grain 2 shows the presence of a low-angle grain boundary of 0.32°. In grain 3, several resolvable subpeaks are observed that can be globally interpreted as reflecting a misorientation of 0.30°, and a similar situation exists in grain 4. The streaking in grain 1 suggests a strain gradient corresponding to a

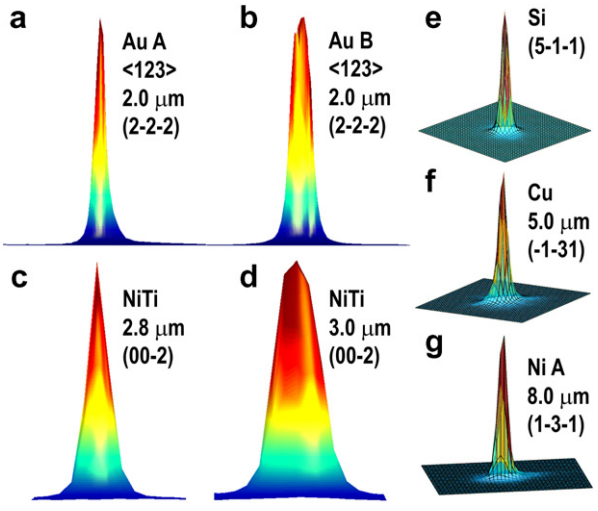

Figure 3. The difference in peak broadening in streaked Au⟨1 2 3⟩ and streaked NiTi peaks in Figure 2a–d; an Si reference peak in 2e compared to non-streaked Cu and Ni peaks in 2f and 2g, respectively.

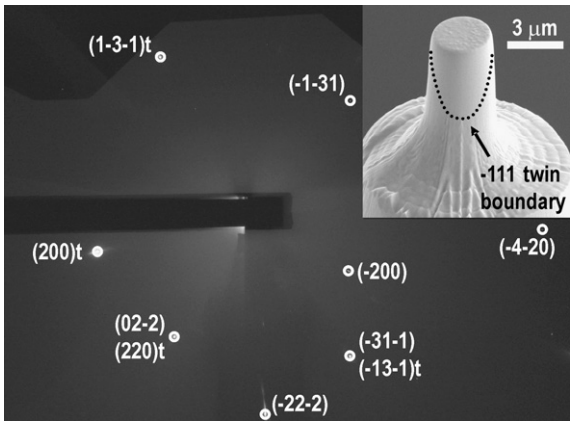

Figure 4. Laue pattern from a 3 μm Au⟨3 4 6⟩ pillar showing both normal (hkl) and $[\bar{1}\,1\,1]$ twin (hkl)t reflections, with an SEM image that displays schematically the orientation of the $[\bar{1}\,1\,1]$ twin boundary.

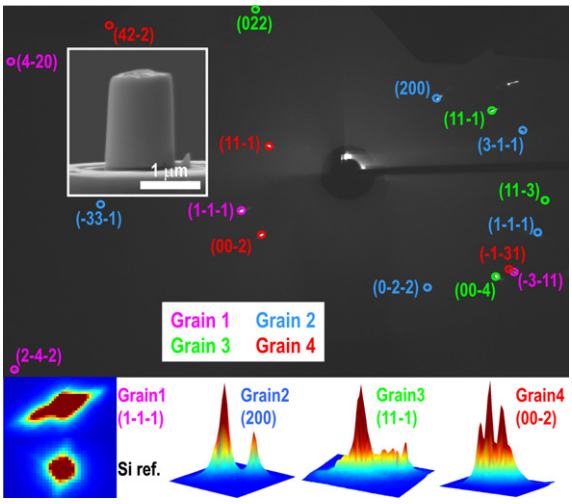

Figure 5. A Laue pattern from a multi-grained Au micropillar, which is displayed as an inset. Below are shown, for grain 1, a two-dimensional image of the $(1\bar{1}\bar{1})$ peak in comparison with a Si reference peak and, for grains 2–4, three-dimensional images of split diffraction peaks.

lattice curvature of ~0.18° and is directly compared in two dimensions with the Si reference that was placed next to the sample. Knowing that these pillars are FIB milled out of an Au film that was sputtered on a Cr substrate (misfit δ $Cr_{\langle 100\rangle\langle 001\rangle}\|Au_{\langle 110\rangle\langle 111\rangle} = 1.806\%$), the observed microstructural details can be explained in part by typical coherency strains formed during sputtering [21]. Such misorientations have not been observed in prior Laue analysis performed on pillars made from the same thin film [13], where the resolution of the system is identical to the one used here (~0.06°). In fact, isotropic peak shapes are reported. However, a line scan in the radial direction showed an FWHM of 0.44° for the $(\bar{3}11)$ reflection, which is substantially larger than the instrumental resolution reported in Ref. [13]. Additionally, this width is larger than the size of the peak splits and the width of unsplit peaks (0.19°) observed in the current work on the same material.

In summary, white beam Laue microdiffraction was used to show a variety of initial microstructural defects from a set of 16 metallic micropillars. From this collection of data it could be shown that strain gradients predominantly exist in smaller samples, with diameters smaller than 5 μm. The identical FIB sputtering conditions for each sample set do not indicate a clear connection between defect structures and ion damage, but nevertheless suggest that the higher surface to volume ratio in smaller pillars increases the occurrence of pre-existing strain gradients. Peak splits and hence GNBs have been found in seven out of the 14 samples—one in a larger pillar (>4 μm) and six in the smaller ones—with strongly increasing misorientation for smaller diameters. The presence of twins suggests that thorough investigations prior to mechanical testing are needed, since SEM imaging cannot easily reveal boundaries. The results presented put the published mechanical data, which are known to contain large scatter, into another context. It is to be expected that the reported scattering among the data published for similar pillars is in part due to the presence of microstructural features that result in classical hardening, because of strain gradient plasticity or dislocation pile-up against GNBs. The existence of these defects does not explain the reported mechanical size effect, but needs to be taken into account before establishing theoretical frameworks. So far, only Laue microdiffraction is capable of excluding the microstructural uncertainties in metallic micropillars for microcompression testing.

The authors thank W.D. Nix, M.D. Uchic, C.P. Frick, D. Kiener and C.A. Volkert for providing the Au, Ni⟨123⟩, NiTi⟨210⟩, Cu⟨421⟩, and Au⟨123⟩ and Au⟨346⟩ samples, respectively. HVS thanks the Swiss National Science Foundation (No. SNF-2100-065152.01, SNF-200020-116283/1) and the European Commission (6th Framework) for financial support of the project NANOMESO. The authors also thank D. Grolimund and M. Willimann, from the MicroXAS beam line at the Swiss Light Source, for technical support.

[1] M.D. Uchic, D.M. Dimiduk, Mater. Sci. Eng. A 400–401 (2005) 268.
[2] M.D. Uchic, D.M. Dimiduk, J.N. Florando, W.D. Nix, Science 305 (2004) 986.
[3] J.R. Greer, W.D. Nix, Phys. Rev. B 73 (2006) 245410.
[4] J.R. Greer, C.R. Weinberg, W. Cai, Mater. Sci. Eng. A (2008), doi:10.1016/j.msea.2007.08.093.
[5] D.M. Dimiduk, M.D. Uchic, T.A. Parthasarathy, Acta Mater. 53 (2005) 4065.
[6] C.P. Frick, B.G. Clark, S. Orso, A.S. Schneider, E. Arzt, Mater. Sci. Eng. A (2007), doi:10.1016/j.msea.2007.12.038.
[7] K.S. Ng, A.H.W. Ngan, Acta Mater. (2008), doi:10.1016/j.actamat.2007.12.016.
[8] F.F. Ciskor, C. Motz, D. Weygand, M. Zaiser, S. Zapperi, Science 318 (2007) 251.
[9] R. Maaß, S. Van Petegem, H. Van Swygenhoven, P.M. Derlet, C.A. Volkert, D. Grolimund, Phys. Rev. Lett. 99 (2007) 145505.
[10] R. Maaß, S. Van Petegem, D. Grolimund, H. Van Swygenhoven, M.D. Uchic, Appl. Phys. Lett. 91 (2007) 131909.
[11] D. Kiener, M. Rester, S. Scheriau, B. Yang, R. Pippan, G. Dehm, Int. J. Mater. Res. 98 (2007) 1047.
[12] C.P. Frick, S. Orso, E. Arzt, Acta Mater. 55 (2007) 3845.
[13] A.S. Budiman, S.M. Han, J.R. Greer, N. Tamura, J.R. Patel, W.D. Nix, Acta Mater. 56 (2007) 602.
[14] C.A. Volkert, E.T. Lilleodden, Philos. Mag. 86 (2006) 5567.
[15] J.F. Nye, Acta Metall. 1 (1953) 153.
[16] M.F. Ashby, Philos. Mag. 21 (1970) 399.
[17] R.I. Barabash, G.E. Ice, F.J. Walker, J. Appl. Phys. 93 (2003) 1457.
[18] D. Kuhlmann-Wilsdorf, N. Hansen, Scripta Metall. Mater. 25 (1991) 1557.
[19] W.D. Nix, H. Gao, J. Mech. Phys. Solids 46 (1998) 411.
[20] K.A. Afanasyev, F. Sansoz, Nano Lett. 7 (2007) 2056.
[21] C.V. Thompson, Annu. Rev. Mater. Sci. 30 (2000) 159.